Sod1 integrates oxygen availability to redox regulate NADPH production and the thiol redoxome

Claudia Montllor-Albalate[a], Hyojung Kim[a], Anna E. Thompson[a], Alex P. Jonke[b], Matthew P. Torres[a,b,c,1], and Amit R. Reddi[a,b,c,1]

[a]School of Chemistry and Biochemistry, Georgia Institute of Technology, Atlanta, GA 30332; [b]School of Biological Sciences, Georgia Institute of Technology, Atlanta, GA 30332; and [c]Parker Petit Institute for Bioengineering and Biosciences, Georgia Institute of Technology, Atlanta, GA 30332

Edited by Michael Karin, Department of Pharmacology, University of California San Diego, La Jolla, CA; received November 9, 2020; accepted November 14, 2021

Cu/Zn superoxide dismutase (Sod1) is a highly conserved and abundant antioxidant enzyme that detoxifies superoxide ($O_2^{\bullet-}$) by catalyzing its conversion to dioxygen (O_2) and hydrogen peroxide (H_2O_2). Using *Saccharomyces cerevisiae* and mammalian cells, we discovered that a major aspect of the antioxidant function of Sod1 is to integrate O_2 availability to promote NADPH production. The mechanism involves Sod1-derived H_2O_2 oxidatively inactivating the glycolytic enzyme, GAPDH, which in turn reroutes carbohydrate flux to the oxidative phase of the pentose phosphate pathway (oxPPP) to generate NADPH. The aerobic oxidation of GAPDH is dependent on and rate-limited by Sod1. Thus, Sod1 senses O_2 via $O_2^{\bullet-}$ to balance glycolytic and oxPPP flux, through control of GAPDH activity, for adaptation to life in air. Importantly, this mechanism for Sod1 antioxidant activity requires the bulk of cellular Sod1, unlike for its role in protection against $O_2^{\bullet-}$ toxicity, which only requires <1% of total Sod1. Using mass spectrometry, we identified proteome-wide targets of Sod1-dependent redox signaling, including numerous metabolic enzymes. Altogether, Sod1-derived H_2O_2 is important for antioxidant defense and a master regulator of metabolism and the thiol redoxome.

oxygen sensing | superoxide dismutase | redox signaling | glycolysis | pentose phosphate pathway

Superoxide dismutases (SODs) serve on the frontline of defense against reactive oxygen species (ROS). SODs, which detoxify $O_2^{\bullet-}$ by catalyzing its disproportionation into O_2 and hydrogen peroxide (H_2O_2), are unique among antioxidant enzymes in that they also produce a ROS byproduct. While much is known about the necessity of scavenging $O_2^{\bullet-}$, it is less clear what the physiological consequences of SOD-derived H_2O_2 are. Paradoxically, increased expression of Cu/Zn SOD (Sod1), which accounts for the majority of SOD activity in cells (1), is associated with reduced cellular H_2O_2 levels (2), suggesting there may be additional unknown mechanisms underlying Sod1 antioxidant activity.

The cytotoxicity of $O_2^{\bullet-}$ stems from its ability to oxidize and inactivate [4Fe-4S] cluster-containing enzymes, which results in defects in metabolic pathways that utilize [4Fe-4S] proteins and Fe toxicity due to its release from damaged Fe/S clusters (3–6). The released Fe can catalyze deleterious redox reactions and, in particular, production of hydroxyl radicals ($^{\bullet}OH$) via Haber-Weiss and Fenton reactions, which indiscriminately oxidizes lipids, proteins, and nucleic acids (4, 7). The importance of Sod1 in oxidative stress protection is underscored by reduced proliferation, decreased lifespan, and numerous metabolic defects, including cancer, when *SOD1* is deleted in various cell lines and organisms (7–11). It was previously proposed that Sod1 limits its steady-state H_2O_2 levels because of its ability to prevent the $O_2^{\bullet-}$-mediated oxidation of Fe/S clusters, which results in the concomitant formation of H_2O_2 (2, 12, 13). However, since vanishingly small amounts of Sod1 (<1% of total cellular Sod1) is sufficient to protect cells against $O_2^{\bullet-}$ toxicity, including oxidative inactivation of Fe/S enzymes (14–16), any changes in Sod1 expression would not be expected to alter H_2O_2 arising from $O_2^{\bullet-}$ oxidation of Fe/S clusters. How then can Sod1, an enzyme that catalyzes H_2O_2 formation, act to reduce cellular [H_2O_2]?

Two previously reported but unexplained metabolic defects in *sod1*Δ strains of *Saccharomyces cerevisiae* point to a potential role for Sod1 in regulating the production of NADPH, a key cellular reductant required for reductive biosynthesis and the reduction and regeneration of H_2O_2 scavenging thiol peroxidases (17) and catalases (18, 19). Yeast strains lacking *SOD1* exhibit increased glucose consumption (20) and defects in the oxidative phase of the pentose phosphate pathway (oxPPP) (21), the primary source of NADPH. Inhibition of key rate-limiting enzymes in glycolysis—including phosphofructose kinase (22), GAPDH (23, 24), and pyruvate kinase (25, 26)—reduces glucose uptake (27–29) and increases the concentration of glucose-6-phosphate (G6P), a glycolytic intermediate that is also the substrate for the first enzyme in the oxPPP, G6P dehydrogenase (G6PDH), which in turn increases oxPPP flux and NADPH production (30–35). Taking these data together, we surmised that Sod1 negatively regulates a rate-determining enzyme in glycolysis, thereby accounting for the observed metabolic defects in glucose utilization and the oxPPP in *sod1*Δ cells (20, 21).

GAPDH, which catalyzes a rate-determining step in glycolysis (36, 37), is very abundant (38), and contains a H_2O_2-reactive

Significance

Cu/Zn superoxide dismutase (Sod1) is a key antioxidant enzyme, and its importance is underscored by the fact that its ablation in cell and animal models results in oxidative stress; metabolic defects; and reductions in cell proliferation, viability, and lifespan. Curiously, Sod1 detoxifies superoxide radicals ($O_2^{\bullet-}$) in a manner that produces an oxidant as byproduct, hydrogen peroxide (H_2O_2). While much is known about the necessity of scavenging $O_2^{\bullet-}$, it is less clear what the physiological roles of Sod1-derived H_2O_2 are. We discovered that Sod1-derived H_2O_2 plays an important role in antioxidant defense by stimulating the production of NADPH, a vital cellular reductant required for reactive oxygen species scavenging enzymes, as well as redox regulating a large network of enzymes.

Author contributions: C.M.-A., H.K., A.E.T., A.P.J., M.P.T., and A.R.R. designed research; C.M.-A., H.K., A.E.T., and A.P.J. performed research; C.M.-A. contributed new reagents/analytic tools; C.M.-A., H.K., A.E.T., M.P.T., and A.R.R. analyzed data; and C.M.-A., M.P.T., and A.R.R. wrote the paper.

The authors declare no competing interest.

This article is a PNAS Direct Submission.

[1]To whom correspondence may be addressed. Email: mtorres35@gatech.edu or amit.reddi@chemistry.gatech.edu.

This article contains supporting information online at http://www.pnas.org/lookup/suppl/doi:10.1073/pnas.2023328119/-/DCSupplemental.

Published December 30, 2021.

catalytic Cys ($k \sim 10^2$ to 10^3 $M^{-1}s^{-1}$), represents a critical redox regulated node that can toggle flux between glycolysis and the oxPPP (32). As such, we hypothesized that a novel aspect of the antioxidant activity of Sod1 is to oxidatively inactivate GAPDH using Sod1-catalyzed H_2O_2, which would in turn stimulate NADPH production via the oxPPP and enhance cellular peroxide scavenging by thiol peroxidases. This mechanism for Sod1-mediated antioxidant activity would explain a number of prior observations, including the findings that elevated Sod1 expression decreases peroxide levels and loss of *SOD1* increases glucose consumption and attenuates oxPPP activity. In addition, more generally, since Sod1-derived H_2O_2 has previously been implicated in the redox regulation of other enzymes, including protein tyrosine phosphatases (39) and casein kinases (15, 16, 40), we also sought to identify proteome-wide redox targets of Sod1.

In the present report we provide evidence highlighting an antioxidant function for Sod1-derived H_2O_2 in integrating O_2 availability to control NADPH production to support aerobic growth and metabolism. The mechanism involves the conversion of O_2 to $O_2^{\bullet-}$ by mitochondrial respiration and an NADPH oxidase, followed by the Sod1-catalyzed conversion of $O_2^{\bullet-}$ to H_2O_2, which in turn oxidatively inactivates GAPDH. The inhibition of GAPDH serves to reroute metabolism from glycolysis to the oxPPP in order to maintain sufficient NADPH for metabolism in air. The aerobic oxidation of GAPDH is dependent on and rate-limited by Sod1, suggesting that it provides a privileged pool of peroxides to inactivate GAPDH under physiological conditions. Finally, we revealed a larger network of cysteine-containing proteins that are oxidized in a Sod1-dependent manner using mass spectrometry-based redox proteomics approaches. Altogether, these results highlight a mechanism for O_2 sensing and adaptation, reveal an important but previously unknown antioxidant role of Sod1 that goes beyond $O_2^{\bullet-}$ scavenging to include the stimulation of aerobic NADPH production, and places Sod1 as a master regulator of proteome-wide thiol oxidation and multiple facets of metabolism.

Results

Sod1 Regulates Glycolysis. In many eukaryotes, including *S. cerevisiae*, glucose uptake negatively correlates with pO_2 (41–44). Indeed, we find that batch cultures of WT yeast cells grown anaerobically consume more glucose per cell than aerobically grown cultures (Fig. 1*A*). Media glucose concentration is plotted versus cell density, rather than time, to correct for differences in growth rate (*SI Appendix*, Fig. S1 *A* and *B*). Consistent with previous studies (20), aerobic cultures of *sod1*Δ strains consume more glucose than WT cells (Fig. 1*A*). However, in the absence of oxygen, both WT and *sod1*Δ cells consume similar amounts of glucose (Fig. 1*A*).

Since defects in glycolytic enzymes, including hexokinase 2 or GAPDH, decrease glucose uptake (27, 28), we sought to determine if the increased glucose consumption of *sod1*Δ cells was associated with altered glycolytic flux. Cytosolic pH is a reporter of glycolytic activity and can be monitored using the GFP-based ratiometric pH sensor, pHluorin. Supplementing glucose-starved WT yeast with glucose results in a rapid decrease in pH due to proton release from glycolytic phosphorylation reactions (Fig. 1 *B* and *C*, phase 1) (45), followed by a slower realkalization phase due to activation of Pma1, a cell surface H^+-ATPase that pumps H^+ into the extracellular space (Fig. 1 *B* and *C*, phase 2) (45). In response to glucose, *sod1*Δ cells exhibit more rapid rates of intracellular acidification, indicating that glycolysis is more active compared to WT cells. In contrast, *sod1*Δ cells exhibit a diminished rate of realkalization, indicating that Pma1 is less active in response to glucose, which is consistent with prior work that found that *sod1*Δ cells exhibit a defect in Pma1 activity (16, 46). To rule out that the intracellular acidification phase is affected by Pma1-dependent realkalization, glucose-dependent changes in intracellular pH were monitored in a strain expressing a hypomorphic allele of PMA1, *pma1-tap*, containing a C-terminal tandem affinity purification (TAP)-tag (*SI Appendix*, Fig. S1*C*). In *pma1-tap* cells, the rate of glucose-induced acidification is similar to WT cells (Fig. 1*C*, phase 1), but there is a significant decrease in the rate of realkalization (Fig. 1*C*, phase 2). Taken together, the data demonstrate that Sod1 negatively regulates glucose uptake and glycolytic activity.

Sod1 Interacts with and Regulates GAPDH Oxidation and Activity. We hypothesized that Sod1-derived H_2O_2 may negatively regulate glucose uptake and glycolytic activity through the oxidative inactivation of GAPDH, which catalyzes a rate-determining step in glycolysis and contains a peroxide-sensitive active site Cys (23). *S. cerevisiae* encodes three GAPDH isoforms—*TDH1*, *TDH2*, and *TDH3*—with *TDH3* being the most highly expressed in log-phase cultures, accounting for >50% of total cellular GAPDH (47). Yeast GAPDH has only two cysteines, catalytic C150 and C154, which sensitizes C150 to oxidation by H_2O_2 (*SI Appendix*, Fig. S1*D*). In order to probe the Sod1-dependence of GAPDH oxidation, we employed a thiol alkylation assay that exploits the reactivity of methoxypolyethylene glycol maleimide (mPEG-mal) with reduced but not oxidized thiols (48). The extent of GAPDH labeling with mPEG-mal, which is 5 kDa, is assessed by determining the changes in electrophoretic mobility of PEGylated GAPDH, corresponding to single- and double-labeled GAPDH at reduced C150 and/or C154 (Fig. 1*D* and *SI Appendix*, S1 *E* and *F*). Thus, the fraction of GAPDH oxidized in vivo can be determined by quantifying the ratio of the intensity of unlabeled GAPDH (oxidized GAPDH) to total GAPDH (*SI Appendix*, Fig. S1 *F–O*). The mPEG-mal approach was validated by treating cells with H_2O_2 and observing a twofold increase in GAPDH oxidation (*SI Appendix*, Fig. S1 *F* and *G*). Moreover, the identity of the specific sites of mPEG-mal labeling was confirmed by observing that a yeast strain expressing a single allele of $Tdh3^{C154S}$ was found to have only two GAPDH proteoforms corresponding to single and unlabeled GAPDH (*SI Appendix*, Fig. S1*P*).

To determine if Sod1 oxidizes GAPDH in vivo, we analyzed GAPDH PEGylation in *sod1*Δ cells expressing empty vector (EV) (*sod1*Δ + EV) or WT *SOD1* (*sod1*Δ + *SOD1*). *sod1*Δ + EV cells exhibit an increase in mPEG-mal labeling compared to *sod1*Δ + *SOD1* cells (Fig. 1 *D* and *E* and *SI Appendix*, Fig. S2 *A* and *B*), indicating that GAPDH is more oxidized in cells expressing *SOD1*. Analysis of 17 replicates over 6 independent trials revealed that expression of *SOD1* results in an approximately twofold increase in GAPDH oxidation, with the median and average GAPDH oxidation in cells expressing *SOD1* being 26% and 35%, respectively, and 13% and 16%, respectively, in cells lacking *SOD1* (Fig. 1*E*). The values of GAPDH oxidation in *SOD1* expressing cells are on par with prior studies of glucose-grown WT yeast that found GAPDH is 26% oxidized (49). Due to variations in the absolute values of GAPDH oxidation across multiple trials (Fig. 1*E*), subsequent comparisons of GAPDH oxidation involved normalizing GAPDH oxidation to that of *SOD1*-expressing cells within each trial, though absolute values are indicated in *SI Appendix*.

In order to assess the extent to which Sod1 mediates the reversible oxidation of GAPDH, we employed an mPEG-mal labeling scheme that involved first capping free GAPDH thiols with *N*-ethylmaleimide, followed by DTT reduction of reversibly oxidized thiols and labeling them with mPEG-mal (*SI Appendix*, Fig. S2 *C–G*). Using this strategy, it was similarly found that Sod1 accounts for an approximately twofold increase in reversible GAPDH oxidation, with three independent trials giving an average GAPDH oxidation value of ~50% in *SOD1* expressing cells and 25% in cells lacking *SOD1* (*SI Appendix*, Fig. S2 *C–G*).

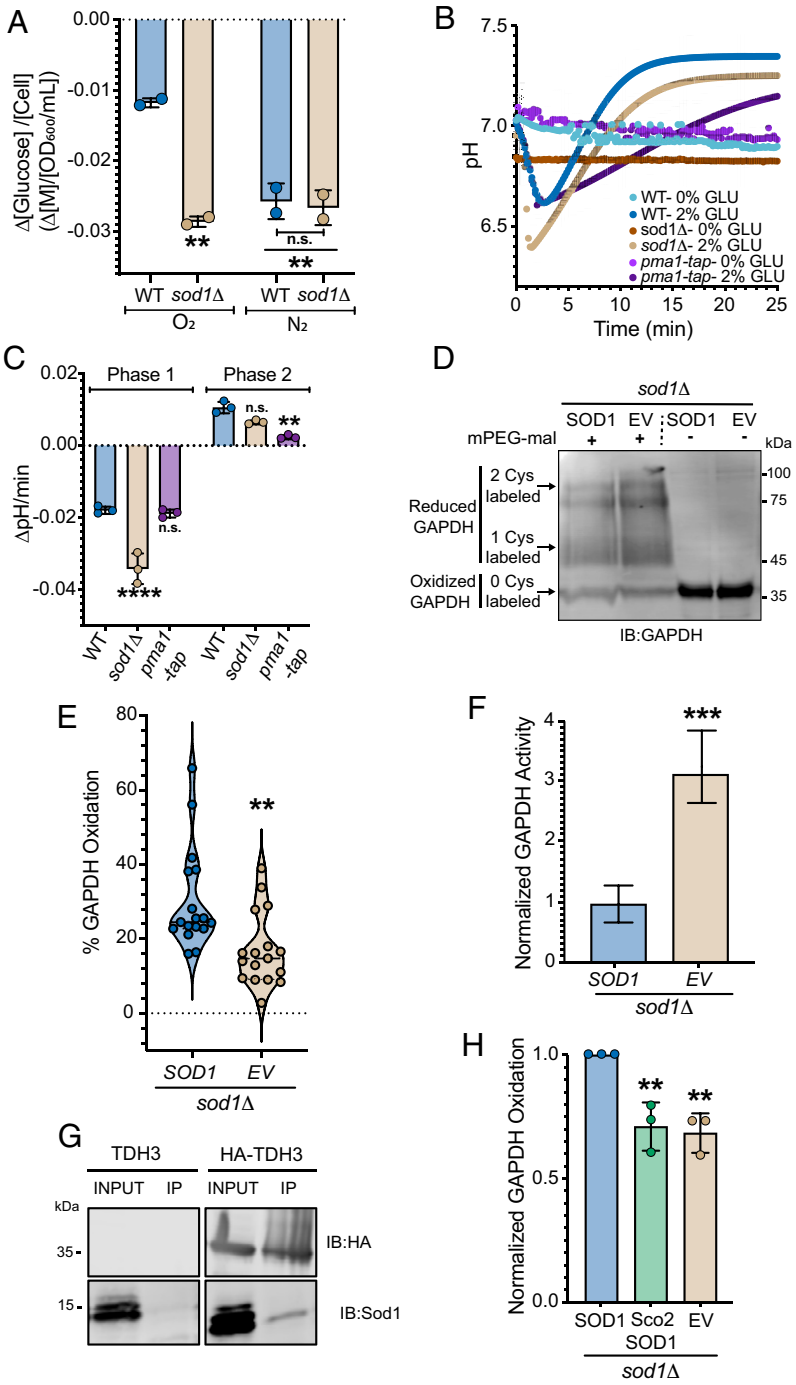

Fig. 1. Cytosolic Sod1 interacts with and regulates glycolysis via the redox regulation of GAPDH. (*A*) Glucose consumption per cell for WT and *sod1*Δ cells grown aerobically (O_2) or anaerobically (N_2). The data are derived from the slope of the linear regions of plots measuring extracellular glucose as a function of culture density (*SI Appendix*, Fig. S1*A*). The data represent the average ± SD from two biological replicates. See also *SI Appendix*, Fig. S1*B*. (*B* and *C*) Time-resolved intracellular pH measurements of glucose starved cells upon pulsing WT, *sod1*Δ, or *pma1*-tap cells expressing a GFP-based pH sensor, pHluorin, with 2% or 0% glucose (GLU) (*B*). The cytosolic acidification rate, a proxy for glycolytic activity (phase 1), and the rate of realkalization of the cytosol, a proxy for Pma1 activity (phase 2), is shown for the indicated strains (*C*). The data represent the average ± SD from triplicate cultures. See also *SI Appendix*, Fig. S1*C*. (*D* and *E*) Analysis of Sod1-dependent GAPDH oxidation as assessed by labeling reduced GAPDH with thiol reactive mPEG-mal. (*D*) Representative immunoblot of GAPDH–mPEG-mal adducts in *sod1*Δ cells expressing yeast Sod1 (SOD1) or EV cultured in 2% GLU. (*E*) The difference in GAPDH oxidation in the indicated strains as assessed by quantifying the ratio of unlabeled GAPDH (oxidized GAPDH) to total GAPDH, both labeled (reduced GAPDH) and unlabeled GADPH. $n = 17$ from 6 independent experimental trials. (*F*) Measurements of GAPDH enzymatic activity in *sod1*Δ cells expressing SOD1 or EV. Data represent the average ± SD from quadruplicate cultures. See *SI Appendix*, Fig. S3 *A* and *B* for representative kinetics traces. (*G*) Lysates from *tdh1*Δ *tdh2*Δ *tdh3*Δ cells expressing HA-Tdh3 or Tdh3 were subjected to IP using α-HA antibody and the IP material was analyzed by immunoblot (IB) using α-HA or α-Sod1 antibody. The data are representative of three independent trials with another replicate shown in *SI Appendix*, Fig. S2*I*. Experimental details are presented in *SI Appendix*, *SI Materials and Methods*. (*H*) Assessment of GAPDH oxidation in *sod1*Δ cells expressing yeast Sod1 (SOD1), mitochondrial IMS targeted Sod1 (Sco2-SOD1), or EV. See *SI Appendix*, Fig. S3 *F* and *G* for representative mPEG-mal immunoblots and quantification of percent GAPDH oxidation. Data represent the average ± SD from three independent trials. The statistical significance is indicated by asterisks using two-tailed Student's *t* tests for pairwise comparisons (*E* and *F*) or by one-way ANOVA for multiple comparisons with Dunett's post hoc test (*A*, *C* and *H*): $^{**}P < 0.01$, $^{***}P < 0.001$, $^{****}P < 0.0001$, n.s., not significant.

In addition, >95% of GAPDH is reducible and alkylatable in both WT and *sod1*Δ cells, indicating that differences in apparent GAPDH oxidation are not due to variations in the ability to reduce and alkylate GAPDH in the two strains (*SI Appendix*, Fig. S2*H*).

We next found that Sod1 interacts with and regulates GAPDH activity. GAPDH catalyzes the oxidative phosphorylation of GAP to 1,3 BPG and requires Cys^{150} for activity. Cells lacking *SOD1* (*sod1*Δ + EV) exhibit threefold greater GAPDH activity (Fig. 1*F* and *SI Appendix*, Fig. S3 *A* and *B*), which correlates with the approximately twofold decrease in GAPDH thiol oxidation relative to *SOD1*-expressing cells (Fig. 1 *D* and *E*). Moreover, GAPDH and Sod1 interact in vivo as assessed by coimmunoprecipitation (co-IP) experiments (Fig. 1*G* and *SI Appendix*, Fig. S2*I*). IP of HA-Tdh3 using anti-HA antibody resulted in the detection of Sod1 by immunoblotting. In contrast, a control strain expressing untagged Tdh3 did not result in co-IP of Sod1, indicating that the apparent interaction between Sod1 and GAPDH is not due to Sod1 nonspecifically binding to the anti-HA resin.

Sod1-mediated GAPDH oxidation is not dependent on the carbon source. Galactose is a fermentable carbon source that alleviates glucose-mediated respiration repression, resulting in more mitochondrial respiratory activity (16). The absolute and relative amounts of GAPDH oxidation in *sod1*Δ + EV and *sod1*Δ + *SOD1* cells cultured in 2% galactose is similar to cells cultured in 2% glucose (*SI Appendix*, Fig. S3 *C–E*).

The effect of Sod1 localization on GAPDH oxidation was also evaluated. Sod1 is primarily cytosolic but is also present in the mitochondrial intermembrane space (IMS). *sod1*Δ cells expressing an IMS-targeted allele of *SOD1*, Sco2-SOD1 (15, 16, 50), exhibit comparable GAPDH oxidation to *sod1*Δ + EV cells, both of which are significantly lower than cells expressing WT *SOD1* (Fig. 1*H* and *SI Appendix*, Fig. S3 *F* and *G*). Altogether, these results indicate that extramitochondrial Sod1 interacts with and oxidatively inactivates GAPDH, thereby explaining the previous observations that *sod1*Δ cells exhibit increased glucose uptake (Fig. 1*A*) and glycolytic activity (Fig. 1 *B* and *C*).

Yno1 and Mitochondrial Respiration Are Sources of Superoxide for GAPDH Oxidation. Sod1 requires a superoxide source to catalyze peroxide production for the control of GAPDH oxidation and activity. As with higher eukaryotes, two primary sources of superoxide in yeast include mitochondrial respiration and the yeast NADPH oxidase, Yno1 (51). Both sources contribute toward GAPDH oxidation as respiration-deficient rho^0 and *yno1*Δ cells exhibit an approximately threefold lower degree of GAPDH oxidation relative to WT cells and phenocopy the *sod1*Δ mutant (Fig. 2*A* and *SI Appendix*, Fig. S4 *A* and *B*). Furthermore, overexpression of Yno1 on a galactose-inducible promoter (pYES-YNO1, 3%GAL), which resulted in a ∼30% increase in dihydroethidium (DHE)-detectable superoxide (*SI Appendix*, Fig. S4*C*) promoted GAPDH oxidation by twofold as compared to cells expressing EV (pYES2-EV, 0 and 3%GAL) or that were cultured in noninducing media (pYES2-YNO1, 0%GAL) (*SI Appendix*, Fig. S4 *D–F*). In total, these results indicate that both Yno1 and mitochondrial respiration are sources of the superoxide substrate required by Sod1 to drive the H_2O_2-dependent oxidation of GAPDH.

O_2-Dependent GAPDH Oxidation Is Dependent on and Rate-Limited by Sod1. All metabolic sources of superoxide and peroxide are ultimately derived from O_2. We therefore sought to determine if Sod1 is the sole enzymatic adapter that links oxygen availability to the control of GAPDH oxidation and if GAPDH oxidation is rate-limited by Sod1. Toward this end, we first asked if Sod1 mediates O_2-dependent GAPDH oxidation. Since WT Sod1 is transcriptionally and posttranslationally down-regulated in response to hypoxia and anoxia (52–55), we utilized *sod1*Δ cells expressing *ADH1*-driven $Sod1^{P144S}$, which is a mutant previously engineered to constitutively express mature enzymatically active Sod1 even in the absence of O_2 (16, 54). Indeed, the $Sod1^{P144S}$ mutant is enzymatically active in lysates derived from both aerobic and anaerobic cultures, whereas WT Sod1 is only fully active in lysates derived from aerobically cultured cells (Fig. 2*B* and *SI Appendix*, Fig. S4*G*). *sod1*Δ cells expressing WT or $Sod1^{P144S}$ exhibit a nearly twofold decrease in GAPDH oxidation when cultured anaerobically, consistent with the requirement for O_2 as the metabolic origin of superoxide and peroxide (Fig. 2*C* and *SI Appendix*, Fig. S4 *H* and *I*). However, remarkably, the O_2-dependence of GAPDH oxidation is completely lost in cells lacking *SOD1*. Furthermore, we determined that the oxidation of GAPDH is rate limited by Sod1, finding that GAL-regulated titration of Sod1 levels results in a dose-dependent increase in GAPDH oxidation (Fig. 2 *D* and *E* and *SI Appendix*, Fig. S4*J*). Altogether, these results indicate that the aerobic oxidation of GAPDH is dependent on and rate-limited by Sod1. It is also worth noting that there is a certain level of O_2-independent GAPDH oxidation that is not dependent on Sod1, albeit the nature of the oxidant in this case is not known.

Sod1-Mediated Oxidative Inactivation of GAPDH Results in Increased NADPH Production and Oxidative Stress Resistance. We next determined if the Sod1-dependent oxidative inactivation of GAPDH results in rerouting of glycolytic metabolism toward oxPPP to produce NADPH and increase resistance to oxidative stress. Titration of Sod1 expression using a GAL-driven *SOD1* allele results in both a dose-dependent increase in GAPDH oxidation as well as NADPH levels (Fig. 3 *A* and *B* and *SI Appendix*, Fig. S5 *A–F*). Control experiments in which GAL is titrated into cells expressing a non-GAL–driven *SOD1* allele indicate that GAL alone does not alter NADPH levels (*SI Appendix*, Fig. S5*G*). Moreover, *tdh3*Δ cells, which express ∼60% less GAPDH than WT cells (Fig. 3*C* and *SI Appendix*, Fig. S5*H*) (47), exhibit increased NADPH levels (Fig. 3*D*), consistent with the finding that oxidative inactivation of GAPDH increases NADPH.

NADPH is required for the reduction and regeneration of numerous cellular antioxidants. Therefore, we determined if the alterations in Sod1-mediated NADPH production correlated with the oxidation state of Tsa1, a yeast peroxiredoxin that scavenges peroxide and that is maintained in a reduced state using NADPH. Peroxide oxidizes Cys^{47} to a sulfenic acid, which in turn forms a disulfide oxidized dimer with Cys^{170} on another Tsa1 monomer. At high peroxide concentrations, (>250 μM exogenous H_2O_2), Cys^{47} is overoxidized to sulfinylated or sulfonylated states rather than becoming disulfide oxidized. To assess Tsa1 oxidation state, we expressed an N-terminal HA tagged allele of *TSA1* in yeast and ascertained its oxidation state by immunoblotting for monomeric or disulfide oxidized dimeric states of Tsa1 using anti-HA antibodies or sulfonylated states using an anti–Prx-SO_3 antibody. HA-Tsa1 complements the H_2O_2 sensitivity of *tsa1*Δ cells (*SI Appendix*, Fig. S6*A*), and we can assign various proteoforms corresponding to reduced monomeric and reversibly oxidized monomeric and dimeric Tsa1 based on the electrophoretic mobility of HA-Tsa1 and HA-$Tsa1^{C47S}$ expressed in WT and *tsa1*Δ cells on SDS/PAGE gels (*SI Appendix*, Fig. S6 *B–D*). *zwf1*Δ cells lacking G6PD, which catalyzes the first committed step of the oxPPP, exhibited decreased NADPH levels (Fig. 3*E*) and elevated disulfide oxidized Tsa1 dimers (Fig. 3 *F* and *G*), thereby confirming that NADPH limitation results in elevated Tsa1 oxidation. Likewise, *sod1*Δ cells also exhibited increased disulfide oxidized Tsa1 dimer formation (Fig. 3 *F* and *G*).

Since steady-state intracellular peroxide levels are similar between WT, *sod1*Δ, and *zwf1*Δ cells (*SI Appendix*, Fig. S6 *E* and *F*), we ascribe the increased Tsa1 disulfide oxidation as arising from diminished NADPH levels. Surprisingly, for reasons that are unclear at this time, *tsa1*Δ and *sod1*Δ cells also exhibited increased Tsa1 sulfonylation, despite these cells having similar steady-state H_2O_2 as WT cells (*SI Appendix*, Fig. S7 *A–E*).

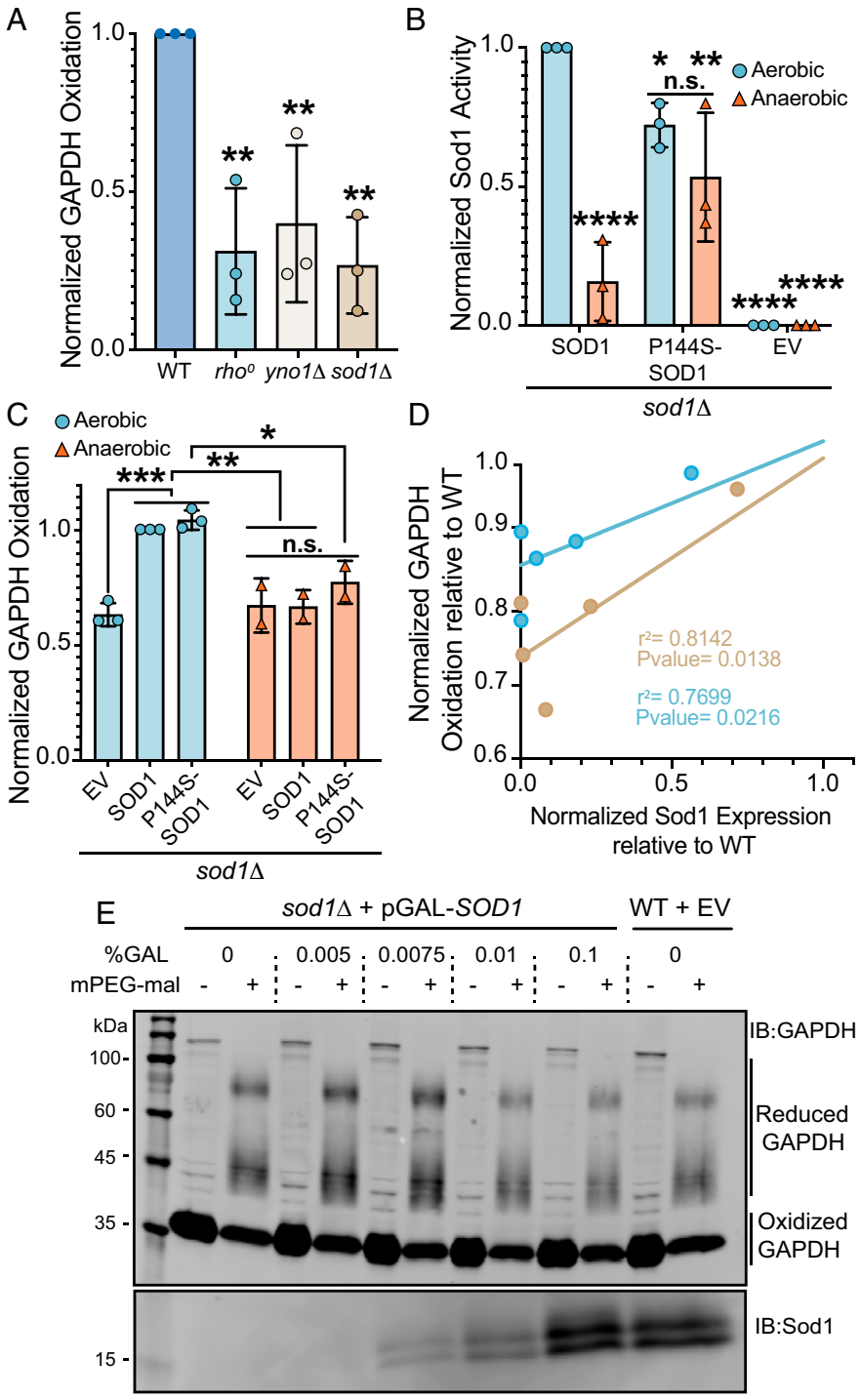

Fig. 2. Aerobic GAPDH oxidation is dependent on and rate-limited by Sod1 and requires Yno1 and mitochondrial respiration as superoxide sources. (*A*) Analysis of GAPDH oxidation as assessed by mPEG-mal labeling of GAPDH in WT, *rho*^{0}, *yno1*Δ, and *sod1*Δ cells cultured in 2% GLU. See *SI Appendix*, Fig. S4 *A* and *B* for representative mPEG-mal immunoblots and quantification of GAPDH oxidation. Data represent the average ± SD from three independent trials. (*B* and *C*) Assessment of the Sod1-dependence on the aerobic oxidation of GAPDH. (*B*) Relative Sod1 activity to assess aerobic and anaerobic Sod1 maturation in *sod1*Δ cells expressing EV, WT SOD1, or the P144S *sod1* mutant. See *SI Appendix*, Fig. S4*G* for representative SOD activity gels and quantification of Sod1 activity. Data represent the average ± SD from three independent cultures. (*C*) Analysis of GAPDH oxidation as assessed by mPEG-mal labeling of GAPDH in aerobic or anaerobic *sod1*Δ cells expressing EV, WT SOD1, or the P144S *sod1* mutant. See *SI Appendix*, Fig. S4 *H* and *I* for representative mPEG-mal immunoblots and quantification of GAPDH oxidation. Data represent the average ± SD from two or three independent trials. (*D* and *E*) Analysis of GAPDH oxidation in WT or *sod1*Δ cells expressing GAL-driven *SOD1* cultured with increasing concentrations of galactose (GAL) (0%, 0.005%, 0.0075%, 0.01% and 0.1% GAL). (*D*) Titration of SOD1 reveals a positive correlation between Sod1 expression and GAPDH oxidation from two independent trials. (*E*) Representative mPEG-mal and Sod1 immunoblot from which the Sod1-dependence of GAPDH oxidation was assessed. In *D*, GAPDH oxidation was normalized to that of the WT cells and the linear regression analysis of the two trials gives coefficients of determination (r^2) of 0.81 and 0.77, with *P* values of 0.01 and 0.02, respectively. See also *SI Appendix*, Fig. S4*J*. The statistical significance relative to WT (*A*) is indicated by asterisks using ordinary one-way ANOVA with Dunett's post hoc test for the indicated pairwise comparison in *A*, $^{**}P < 0.01$. The statistical significance relative to the aerobic SOD1 expressing cells is indicated by asterisks using two-way ANOVA for multiple comparisons with Tukey's post hoc test for the indicated pairwise comparisons in *B* and *C*: $^{*}P < 0.05$, $^{**}P < 0.01$, $^{***}P < 0.001$, $^{****}P < 0.0001$, n.s., not significant.

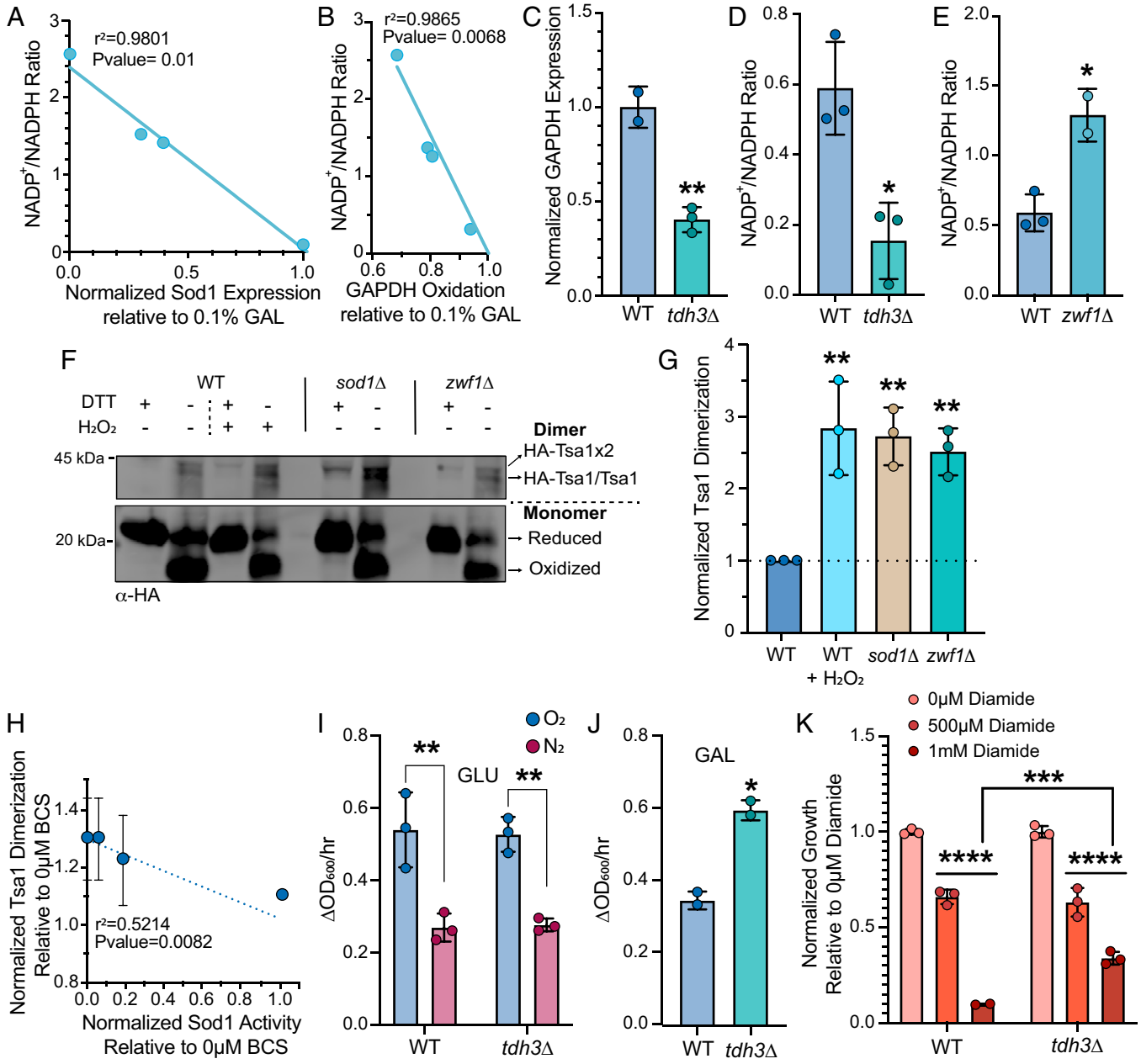

Fig. 3. Sod1-mediated oxidative inactivation of GAPDH results in increased NADPH production and resistance to oxidative stress. (*A* and *B*) Sod1 expression positively correlates with GAPDH oxidation (*A*) and NADPH production (*B*). See *SI Appendix*, Fig. S5*A* for representative immunoblots assessing Sod1 expression and GAPDH oxidation by mPEG-mal labeling in *sod1*Δ cells expressing GAL-driven *SOD1* cultured with increasing concentrations of galactose (GAL) (0.005%, 0.0075%, 0.01%, and 0.1% GAL). The $NADP^+$/NADPH ratio inversely correlates with normalized Sod1 expression (*A*) and GAPDH oxidation (*B*), with linear regression analysis in *A* and *B* giving coefficient of determinations (r^2) of 0.98 and 0.99 and *P* values of 0.01 and 0.007, respectively. See also *SI Appendix*, Fig. S5 *B*–*G* for representative correlation plots between Sod1 expression or GAPDH oxidation and $NADP^+$/NADPH ratio and NADPH concentration. (*C* and *D*) Depletion of intracellular GAPDH decreases the $NADP^+$/NADPH ratio. (*C*) GAPDH expression is reduced by ~60% in *tdh3*Δ cells as assessed by immunoblot analysis (see *SI Appendix*, Fig. S5*H* for representative GPADH immunoblots). (*D*) Measurements of the $NADP^+$/NADPH ratio in WT and *tdh3*Δ. Data represent the average ± SD from triplicate cultures. (*E*) Ablation of G6PD (Zwf1) increases the cellular $NADP^+$/NADPH ratio. Data represent the average ± SD from triplicate cultures. (*F* and *G*) Ablation of Sod1 and Zwf1 increases DTT-reversible disulfide oxidation and dimerization of peroxiredoxin (HA-Tsa1x2). Representative immunoblot of HA-Tsa1 in WT, both treated and untreated with H_2O_2 or DTT, *sod1*Δ, and *zwf1*Δ cells. Tsa1 proteoforms identified include oxidized and reduced monomer and disulfide oxidized dimer (*F*). Quantification of the fraction of disulfide oxidized Tsa1 dimer over the total amount of Tsa1 from three independent trials (*G*). Data represent the average ± SD. Assignment of HA-Tsa1 proteoforms are derived from *SI Appendix*, Fig. S6. (*H*) Sod1 activity inversely correlates w+ith Tsa1 disulfide dimerization. Sod1 activity, as titrated using the copper chelator, BCS, negatively correlates with disulfide dimerized HA-Tsa1. Representative Sod1 activity gel and HA-Tsa1 immunoblot analysis are shown in *SI Appendix*, Fig. S7 *F* and *G*. (*I*–*K*) Aerobic and anerobic growth rates in 2% glucose media (*I*), aerobic growth rate in 2%GAL media (*J*), and diamide sensitivity (*K*) of WT and *tdh3*Δ cells. In *K*, growth after 9 h of exposure to diamide is reported. See *SI Appendix*, Fig. S7 *H* and *I* for complete growth curves. Data represent the average ± SD from triplicate cultures. The statistical significance relative to WT is indicated by asterisks using two-tailed Student's *t* test for pairwise comparisons in *C*, *D*, *E*, and *J*: $*P < 0.05$, $***P < 0.001$. The statistical significance relative to WT (*I*) is indicated by asterisks using ordinary one-way ANOVA with Dunett's post hoc test for the indicated pairwise comparison in *I*, $*P < 0.05$. The statistical significance relative to the aerobic growth rate (*I*) or 0 μM diamide (*K*) is indicated by asterisks using two-way ANOVA for multiple comparisons with Dunett's or Tukey's post hoc test for the indicated pairwise comparisons in *I* and *K*, respectively; $**P < 0.01$, $***P < 0.001$, $****P < 0.0001$.

Titration of a copper chelator, bathocuproinedisulfonic acid (BCS), resulted in a dose-dependent decrease in Sod1 activity, without affecting expression, and consequent increase in the formation of disulfide-dimerized Tsa1 (Fig. 3*H* and *SI Appendix*, Fig. S7 *F* and *G*). Overall, these results are consistent with Sod1 mediated oxidative inactivation of GAPDH promoting NADPH production via the oxPPP, thereby allowing for the regeneration of peroxide scavengers like Tsa1.

In order to determine if the oxidative inactivation of GAPDH by Sod1 provides a physiological benefit for cells, we measured the aerobic growth and oxidative stress resistance of cells expressing low and high levels of GAPDH. Although WT and *tdh3*Δ cells have similar aerobic and anaerobic growth rates in 2% GLU (Fig. 3*I*), when cultured in 2% GAL, a fermentable carbon source that promotes respiration in yeast, *tdh3*Δ cells have a marked enhancement in growth rate compared to WT cells (Fig. 3*J*). Moreover, *tdh3*Δ cells exhibit greater resistance to peroxide (*SI Appendix*, Fig. S7*H*) and diamide induced oxidative stress (Fig. 3*K* and *SI Appendix*, Fig. S7*I*). Altogether, the enhanced aerobic fitness and oxidative stress resistance of cells depleted of GAPDH is consistent with a beneficial role for the Sod1-mediated inactivation of GAPDH.

Sod1 Regulates GAPDH Oxidation in Human Cells. Since both Sod1 and GAPDH are highly conserved, from yeast to humans, we sought to establish if Sod1 regulates GAPDH oxidation in human embryonic kidney HEK293 cells. Human GAPDH has an additional peroxide reactive Cys, which would result in three PEGylated proteoforms, corresponding to triple-, double-, and single-labeled GAPDH in immunoblots (*SI Appendix*, Fig. S8*A*). As expected, cells treated with H_2O_2 exhibited less mPEG-mal labeling, indicating a larger fraction of oxidized GAPDH compared to nontreated cells (*SI Appendix*, Fig. S8 *B* and *C*). To determine if Sod1 promoted GAPDH oxidation, we depleted Sod1 in HEK293 cells using small-interfering RNA against Sod1 (siSOD1) or scrambled control RNAi (siCTRL). Across various trials, we consistently observed a depletion of ∼60 to 80% of Sod1 (*SI Appendix*, Fig. S8 *D* and *E*) and a corresponding decrease in GAPDH oxidation (*SI Appendix*, Fig. S8 *F–H*). Sod1 increases GAPDH by ∼7 to 16%, which is comparable to the contribution observed from exogenous peroxide treatment (*SI Appendix*, Fig. S8*B*). Moreover, as with yeast, we find that Sod1 expression levels across multiple trials positively correlate with GAPDH oxidation (*SI Appendix*, Fig. S8*I*). Notably, the y-intercept of the linear regression (r^2 = 0.76; P = 0.002) is close to 0, indicating that in the complete absence of Sod1, GAPDH oxidation is expected to be ∼0% (*SI Appendix*, Fig. S8*I*). Furthermore, cell lines that overexpress Sod1, such as the breast cancer cell line MCF7 (56), exhibit a nearly threefold increase in GAPDH oxidation compared to HEK293 cells (*SI Appendix*, Fig. S8 *J* and *K*). Altogether, these results indicate that Sod1-mediated oxidation of GAPDH is conserved in humans.

Redox Proteomics Identifies Additional Putative Targets of Sod1 Redox Regulation. The high abundance and broad cellular distribution of Sod1 suggests that it may function as a redox regulator of a broad variety of substrates in addition to GAPDH. To test this, we conducted a high-powered quantitative redox proteomics screen of WT and *sod1*Δ yeast to identify Sod1-dependent redox substrates. We used a combined stable isotope labeling with amino acids in cell culture (SILAC)-tandem mass tags (TMT) approach, whereby *sod1*Δ-dependent changes in protein abundance are quantified through SILAC and changes in reversible cysteine oxidation are quantified through cysteine-reactive iodoacetyl TMT (iodo-TMT) before and after reduction with DTT (Fig. 4*A*) (57). In this case, the same peptide from WT and *sod1*Δ cells is distinguished by a mass shift, allowing quantitative comparison of the peptide's abundance in each strain [protein expression difference = $\log_2(sod1\Delta_{light}/WT_{heavy})$]. Subsequent fragmentation/sequencing of each peptide reveals the peptide/protein identity and, if cysteine is present, releases TMT reporter ions enabling quantification of the cysteine oxidation percentage in each strain (oxidation difference = *sod1*Δ%Ox − WT%Ox) (*Materials and Methods*). Consequently, the study reveals a broad range of proteins that undergo significant changes in abundance, cysteine oxidation, or both (Fig. 4*B* and *SI Appendix*, Fig. S9*A*).

Focusing first on the effects of *SOD1* deletion on proteome-wide protein abundance, we independently analyzed the SILAC mass spectrometry (MS) data. A total of 4,409 proteins were confidently detected and quantified, and ∼9% of these (373) exhibited significant differences in abundance between the two strains (Fig. 4*C* and Dataset S1). Of these, 114 (30.6%) exhibit a significant decrease in protein abundance in *sod1*Δ cells compared to 259 (69.4%) proteins that exhibit a significant increase in abundance. The changes in protein expression reflect known metabolic defects associated with loss of *SOD1*, including alleviation of glucose repression, increased mitochondrial mass, induction of the iron starvation and antioxidant responses, and diminished plasma membrane casein kinase expression (Fig. 4*D* and *SI Appendix*, Fig. S9*B*). Gene ontology (GO) enrichment analysis of proteins undergoing a statistically significant change in abundance revealed a set of outlier ontologies (i.e., GO terms falling outside the 90th percentile in the distribution of fold-enrichment) that could be clustered into discrete bins. Notably, we observed the greatest enrichment for ontologies linked to glycolysis and pentose phosphate pathways. This included chitin synthesis (median fold-enrichment [FE]: 29.6), which feeds directly from D-fructose-6-phosphate, a precursor to the GAPDH substrate D-glyceraldehyde-3-phosphate and a key metabolite in the PPP; cellular polysaccharide catabolism (starch and sucrose catabolism) (FE: 21.1); amino acid biosynthesis (FE: 20.6), which relies on several glycolytic intermediates; as well as purine biosynthesis/metabolism that feeds on D-ribose-5-phosphate from the PPP (FE: 14.1) (Fig. 4*E* and Dataset S1). We observed lower but still significant GO enrichment of proteins involved in redox processes and functions (FE: 14.1), including ontologies encompassing oxidoreductase activity, NADH oxidation, and ROS metabolic processes; and enrichment of proteins associated with ATP synthase/proton pumping (FE: 17.6).

Next, we focused on the effects of *SOD1* deletion on proteome-wide cysteine oxidation as revealed by iodo-TMT MS data. A total of 2,077 cysteine residues were confidently detected ranging in oxidation level from 1 to 100% and a median level of 28.9% across all sites measured. Cross-referencing all sites against protein functional residues revealed 54 of these sites associated with metal binding (38 sites, 74%), active sites (11 sites, 20%), and protein or DNA binding (5 sites, 9%) and cysteine residues involved in these functions also exhibited statistically higher overall oxidation levels in both WT and *sod1*Δ (44.6%, $P < 0.0001$) (*SI Appendix*, Fig. S9*C* and Dataset S1). Mean global oxidation levels were nearly identical between both strains (32.8% vs. 32.9%) (*SI Appendix*, Fig. S9*A*).

Approximately 5% of the quantified cysteine sites (99 sites, 96 proteins) undergo significant changes in oxidation between WT and *sod1*Δ cells, and of these, we found that 65% exhibit reduced oxidation levels in the absence of *SOD1* (Fig. 4*F* and Dataset S1). GAPDH peptides, and C150/C154 specifically, were readily detected but failed to undergo iodo-TMT reporter release under any of the three collision energies used for peptide fragmentation, preventing quantitation of SOD1-dependent oxidation in these experiments. However, we were able to detect DTT-irreversible GAPDH thiol oxidation products, including sulfinic acid (SO_2) and dehydroalanine, and found they were elevated up to 1.6-fold in WT cells relative to *sod1*Δ cells (Dataset S1). These results support the conclusion that Sod1 contributes to both reversible and irreversible GAPDH oxidation as detected

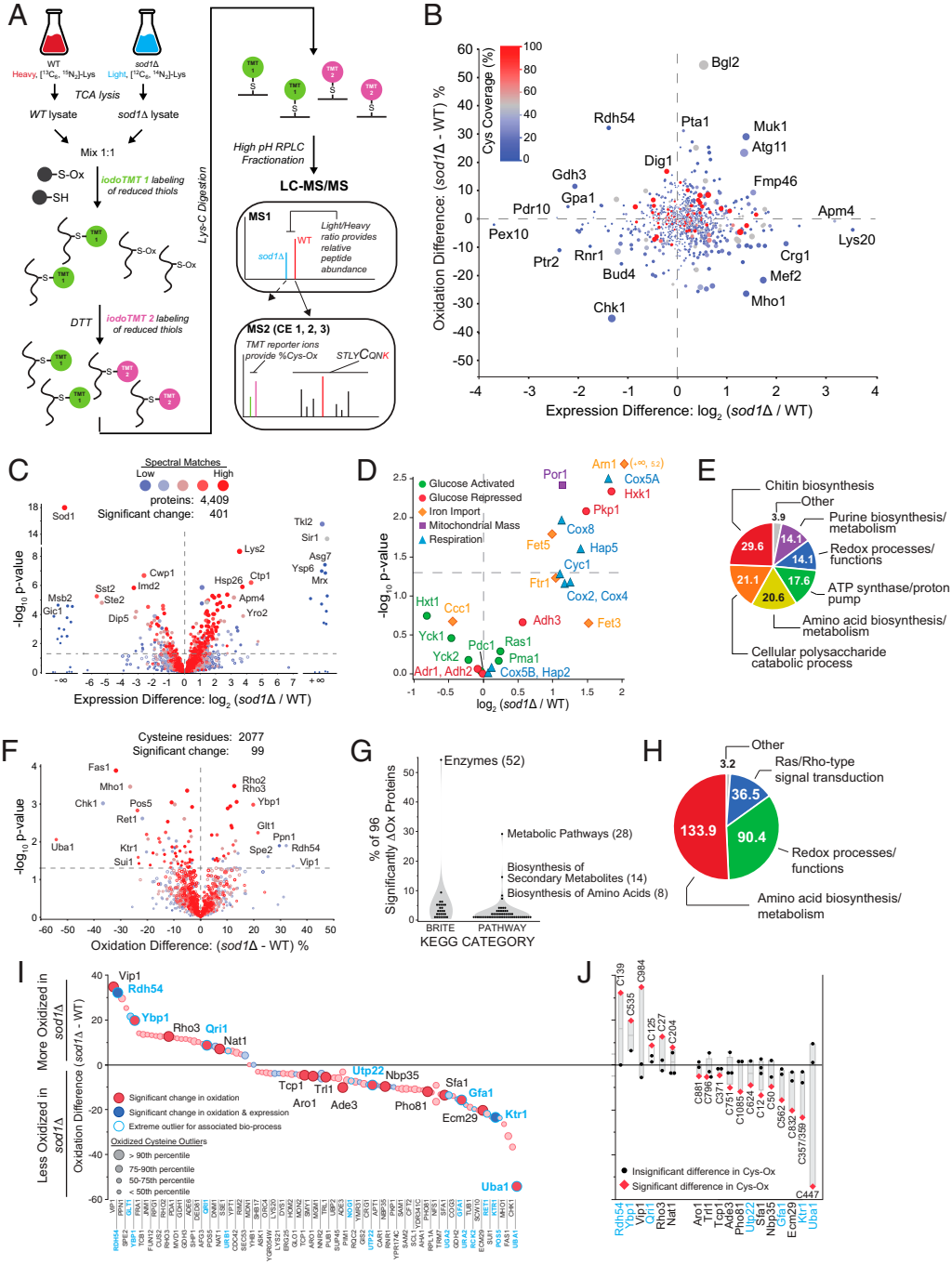

Fig. 4. Redox proteomics identifies additional putative targets of Sod1 redox regulation. (*A*) SILAC-TMT redox proteomics workflow. SILAC labels distinguish the cellular origin of each peptide. Cysteine-reactive and isobaric iodo-TMT reporters, undetectable during the first MS stage (MS1) and released during peptide fragmentation in MS2, enable unique cysteine %oxidation calculation in WT and *sod1*Δ cells. (*B*) Plot of aggregated average cysteine oxidation difference relative to protein expression difference in *sod1*Δ vs. WT cells. Points near the origin (0,0) undergo less change in relative abundance and cysteine oxidation compared to points further from the origin. Cysteine coverage indicates the fraction of cysteine residues detected for each protein. (*C*) Volcano plot of $-\log_{10}(P$ value) relative to protein expression difference [$\log_2$(*sod1*Δ/WT)] calculated from aggregate SILAC data. Proteins above $-\log_{10}(P$ value) 1.3 are significantly different in abundance between the two strains ($P < 0.05$). Positive and negative values of $\log_2$(*sod1*Δ/WT) indicate proteins that are more expressed in *sod1*Δ and WT, respectively. Proteins with a single detected label are indicated as ± infinity. (*D*) Subset of data from *C*, showing expression change for proteins associated with bioprocesses functionally associated with loss of *SOD1*. See also *SI Appendix*, Fig. S9*B*. (*E*) Median FE values for GO bins observed for proteins undergoing greater than twofold change in abundance between *sod1*Δ and WT cells. (*F*) Volcano plot of $-\log_{10}(P$ value) relative to protein expression difference [$\%Ox_{sod1\Delta} - \%Ox_{WT}$] calculated from iodo-TMT data aggregated at the cysteine level. $-\text{Log}_{10}(P$ value) of 1.3 or above indicate significantly different cysteine oxidation between the two strains ($P < 0.05$). See also *SI Appendix*, Fig. S10*A*. (*G*) Kyoto Encyclopedia of Genes and Genomes (KEGG) Brite and Pathway enrichment analysis for the 96 proteins harboring oxidation sites that change significantly in the absence of *SOD1*. Number of associated proteins shown in parentheses. See also *SI Appendix*, Fig. S9*D*. (*H*) Median FE values for GO bins observed for proteins with at least one cysteine undergoing >5% difference in oxidation between WT and *sod1*Δ. (*I*) Rank-ordered plot of cysteine residues from proteins that exhibit statistically significant differences in oxidation between *sod1*Δ and WT. Statistical outliers in oxidation change between strains (circle size) and with respect to other cysteine residues contained within share bioprocess (blue halo, blue text) are indicated. (*J*) Deconvoluted oxidation differences for proteins in which a single cysteine was found to be a statistical outlier from other observed cysteine oxidation sites in the same protein. See also *SI Appendix*, Fig. S10*B*.

by targeted mPEG-mal/GAPDH immunoblotting experiments and MS, respectively.

On average, cysteine residues in *sod1*Δ cells appear to be less oxidized compared to WT cells, consistent with a role for Sod1 in providing a source of peroxides for thiol oxidation. On the other hand, cysteine residues that are more oxidized in *sod1*Δ cells compared to WT may be due to oxidative stress, in part mediated by the decrease in NADPH production due to diminished Sod1-mediated GAPDH oxidation and the subsequent reduction in flux through the oxPPP.

Over half of the proteins harboring the 99 significantly changing oxidation sites are classified as enzymes, with the next most populous class represented at less than 10% in comparison (Fig. 4*G* and Dataset S1). Most of these proteins are also associated with metabolism, synthesis of secondary metabolites, and biosynthesis of amino acids. Clustering of ontologies that were statistical outliers for FE supported these findings and produced three distinct ontology bins. Ontologies associated with amino acid biosynthesis were predominantly enriched (FE: 133.9) and to a far greater extent than what we observed for Sod1-dependent protein abundance changes (Fig. 4*H* and Dataset S1). Moreover, many of the proteins within this bin exhibit reduced oxidation in the absence of *SOD1*, and map to multiple different amino acid biosynthesis/metabolism pathways including those for lysine (Lys20/21), arginine (Car1), threonine (Hom2), and s-adenosyl methionine (Sam1/2), to name a few (*SI Appendix*, Fig. S9 *D* and *E*). Ontologies encompassing redox processes and functions were also highly enriched (FE: 90.4), and include proteins involved in catalysis of redox reactions in which a CH-NH2 group acts as a hydrogen or electron donor and reduces NAD^+ or $NADP^+$. Finally, we also found significant enrichment of proteins involved in Ras and Rho signal transduction (median FE: 36.5), which hint at a unique and unrealized connection between *SOD1*, redox homeostasis, actin mobilization, and cell motility.

Considering the role of Sod1 as a direct regulator of GAPDH through C150 oxidation, we asked whether our proteomic data might contain evidence of a similar relationship between Sod1 and other proteins, wherein: 1) the protein is specifically affected at one out of multiple possible cysteine residues; and 2) oxidation of this cysteine is significantly reduced in the absence of *SOD1*. To create this filter, we binned each of the 99 sites based on whether the change in oxidation was a statistical outlier (>90th percentile) from other cysteine residues in the protein, revealing 18 proteins (Fig. 4 *I* and *J*). In seven of these cases, the change in oxidation was also found to be an outlier with respect to other oxidized cysteine residues found in other proteins within the associated bioprocess for the given protein (Fig. 4*I*, blue halos, *SI Appendix*, Fig. S10*A*, and Dataset S1). Deconvolution of their site-specific changes in oxidation revealed a range of responses reflecting the sensitivity of specific cysteine residues to the presence or absence of *SOD1* (Fig. 4*J*). Some of these coincided with proteins enriched previously through ontology, most notably Sfa1 and Gfa1 involved in pyruvate metabolism and conversion of D-fructose-6-phosphate, respectively. Sfa1-C12 and Gfa1-C562, but not other detected cysteine residues in either protein, undergo a significant decrease in oxidation in the absence of *SOD1* (Dataset S1). We also observed that in one case, Nbp35 (required for maturation of extramitochondrial Fe-S proteins), the site of dynamic oxidation is a functional metal binding site in the protein (Dataset S1). Finally, other proteins not revealed by previous analyses were also evident, most notably Uba1, which is the sole enzyme necessary for activating ubiquitin in yeast. Uba1-C447, which is immediately adjacent to the ATP binding site for the protein, undergoes a large drop in oxidation in the absence of *SOD1*, going from a maximum ~89% in WT cells down to ~28% in *sod1*Δ cells (*SI Appendix*, Fig. S10*B* and Dataset S1). In comparison, C600, which is the site of ubiquitin attachment, undergoes very little change in oxidation upon deletion of *SOD1*. Collectively, these data provide an unparalleled look into the dynamic oxidation of specific cysteine thiols as well as protein abundance changes in response to the loss of *SOD1*.

Discussion

SODs are unusual "antioxidants" in that they catalyze the production of one ROS, H_2O_2, as a byproduct of detoxifying another ROS, $O_2^{\bullet-}$. Herein, we sought to understand if there were physiological roles for Sod1-derived H_2O_2 in redox regulating antioxidant defenses and the thiol proteome. We identified a redox circuit in which Sod1 senses the availability of O_2 via metabolically produced $O_2^{\bullet-}$ radicals and catalyzes the production of H_2O_2 that oxidatively inactivates GAPDH. GAPDH inactivation in turn promotes flux through the oxPPP to generate the NADPH required for aerobic metabolism and antioxidant defenses (30, 31). Moreover, using MS-based redox proteomics approaches, we identified a larger network of proteins whose redox state, like GAPDH, is sensitive to Sod1 levels. Altogether, our results highlight a mechanism for the antioxidant activity of Sod1—namely that Sod1-derived H_2O_2 can stimulate NADPH production—and place Sod1 as a master regulator of the cellular redox landscape through two potential mechanisms: either by providing a direct source of thiol oxidizing H_2O_2 or by altering the NADPH/$NADP^+$ redox balance through the Sod1/GAPDH signaling axis (Fig. 5).

We propose a proximity-based model in which Sod1 provides a highly localized and privileged pool of peroxide capable of physiological GAPDH oxidation and control of glycolytic flux. Since GAPDH and Sod1 are among the most abundant soluble proteins in cells, present at levels >100 μM (58), rapid peroxide diffusion due to short distances between Sod1 and GAPDH, or peroxide channeling due to transient interactions between these proteins may allow for the Sod1-mediated aerobic oxidation of GAPDH. This proximity-model is supported by the observations that Sod1 and GAPDH interact (Fig. 1*G* and *SI Appendix*, Fig. S2*I*), WT and *sod1*Δ cells have similar levels of intracellular peroxide (*SI Appendix*, Fig. S11*A*), and exposure to concentrations of exogenous H_2O_2 up to 0.25 mM, which is sufficient to substantially increase intracellular peroxides (*SI Appendix*, Fig. S11*A*), does not result in GAPDH oxidation (*SI Appendix*, Fig. S11 *B–D*). Altogether, these findings are consistent with a model in which only localized production of H_2O_2 by Sod1 is capable of physiological GAPDH oxidation. Sod1-mediated redox signaling complements other paradigms of peroxide signaling, such as the transfer of oxidizing equivalents through thiol-disulfide exchange (59) or the "flood-gate" effect, which posits that a burst of H_2O_2 inactivates antioxidants like peroxiredoxins so that sufficient peroxide may diffuse far enough to transmit redox signals (60).

How physiologically significant is the Sod1-mediated oxidative inactivation of GAPDH? Prior metabolic flux analysis in yeast found that the inactivation of up to ~20% of the total GAPDH pool does not result in oxPPP rerouting or increase in NADPH (31). In contrast, inactivation of greater than 20% of the GAPDH pool results in substantially increased carbohydrate flux through the oxPPP to elevate NADPH in a manner that has a power dependence on GAPDH oxidation (31). We find herein that in the absence of *SOD1*, GAPDH oxidation is at or below this ~20% threshold. When *SOD1* is expressed, the average and median GAPDH oxidation exceeds 20%, leading to elevated NADPH. Thus, Sod1-derived H_2O_2 ensures that there is sufficient steady-state oxidized GAPDH to enable oxPPP-dependent NADPH production for optimal growth in air. However, it is also possible that there are other redox sensitive nodes that contribute to Sod1-dependent changes in [NADPH] independent of GAPDH.

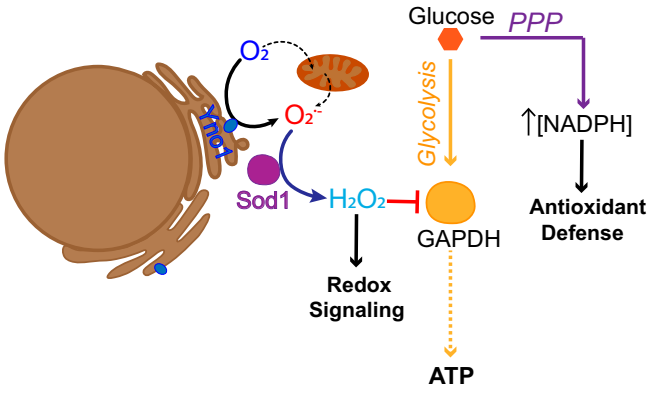

Fig. 5. Proposed model for how Sod1 integrates O_2 availability to regulate GAPDH oxidation and balance flux between glycolysis and the oxPPP to produce NADPH.

The aerobic oxidation of GAPDH is rate-limited by Sod1 (Fig. 2 *D* and *E*), suggesting that the oxidative inactivation of GAPDH and glycolytic flux may be dynamically regulated by Sod1 expression, maturation, which itself is O_2-dependent, its interactions with GAPDH, or posttranslational modifications that regulate Sod1 localization and activity (61–64). With respect to Sod1 posttranslational modifications, it is tempting to speculate that the O_2-sensing redox circuit we identified herein may be integrally linked to the nutrient sensing target of rapamycin (TOR) pathway. TOR-dependent phosphorylation at Ser38 in yeast (Thr39 in humans) suppresses Sod1 activity in response to nutrient abundance to promote cell growth, whereas starvation promotes Sod1 activity (64). TOR/Sod1 signaling may be coupled to the redox regulation of GAPDH and glycolytic flux, thereby providing a means to integrate oxygen and nutrient availability to control metabolism. With respect to Sod1 expression, since many cancer cells overexpress Sod1, it is conceivable that the Sod1/GAPDH signaling axis promotes cancer cell survival and drug resistance due to its potentiation of NAPDH production via the PPP (65). Thus, our work also sheds new light on the benefits of anti-Sod1 therapeutic interventions (64, 66–69). Indeed, we find that the breast cancer MCF-7 cell line exhibits greater levels of GAPDH oxidation relative to HEK293 cells, correlating with its higher levels of Sod1 expression. Like Sod1, MnSOD (Sod2), which is highly inducible, is a biomarker for cancer progression and is involved in the metastasis of certain cancers (70–73). As Sod2 may have its own distinct set of redox targets that control cell metabolism and physiology, therapeutic interventions that target Sod1, Sod2, or both potentially offers a means to titrate mitochondrial and extramitochondrial peroxide-based signaling to combat disease.

The integration of O_2 availability through the Sod1/GAPDH redox signaling axis is dependent on key sources of $O_2^{\bullet-}$, including the yeast NADPH oxidase Yno1 and mitochondrial respiration (Fig. 2). Given that Sod1 and GAPDH are primarily cytosolic enzymes, it is not surprising that we found Yno1, which is localized at the endoplasmic reticulum (ER) membrane and produces $O_2^{\bullet-}$ on the cytosolic side, is required for transducing O_2 availability to the $O_2^{\bullet-}$ signal required for Sod1/GAPDH signaling (51). Indeed, Yno1 was previously found to regulate Sod1-mediated redox regulation of yeast casein kinase Yck1/2 signaling, which also occurs in the cytosol in proximity to the plasma membrane. However, it was rather surprising to find that mitochondrial respiration, as assessed in a respiratory incompetent yeast mutant lacking mitochondrial DNA, could also contribute $O_2^{\bullet-}$ for Sod1-mediated GAPDH oxidation in the cytosol. Complex I (missing in *S. cerevisiae*) and III are the primary sources of electron leakage from the electron transport chain and produce $O_2^{\bullet-}$ in the mitochondrial IMS (74). Yet, IMS-targeted Sod1 does not mediate GAPDH oxidation (Fig. 1*H*). Thus, IMS $O_2^{\bullet-}$, which is charged and membrane impermeable, must exit the mitochondria for Sod1/GAPDH signaling via voltage-dependent anion channels (75) or as membrane-permeable neutral hydroperoxyl radicals ($HO_2^{\bullet}$). Our results highlight how mitochondrial respiration may be an important sensor for O_2, providing a source of $O_2^{\bullet-}$ that can act as a retrograde signal to control extramitochondrial metabolism for adaptation to increasing pO_2. The present study complements prior work that found mitochondrial respiration is a key source of ROS required for adaption to hypoxia via hypoxia inducible factor signaling (76).

The finding that Sod1 can redox regulate GAPDH prompted us to determine if other redox targets of Sod1 exist. Indeed, MS-based redox proteomics identified a number of proteins that, like GAPDH, are more oxidized in the presence of Sod1. Interestingly, enzymes associated with pathways orthogonal to glycolysis and the PPP, namely involved in amino acid biosynthesis, were prominently enriched over other groups (Fig. 4*H* and *SI Appendix*, Fig. S9 *D* and *E*), and suggest that Sod1-dependent growth control may also be modulated through additional targets within these pathways that may have evolved Sod1-sensitive cysteine oxidation sites. On the other hand, all but one of these proteins (Nbp35) are oxidized at Cys residues not associated with a direct role in catalysis or function, raising the possibility that oxidation of such sites may function allosterically. For example, the E1 ubiquitin activating enzyme Uba1 is differentially oxidized at C447 (*SI Appendix*, Fig. S10*B* and Dataset S1), which is immediately adjacent to the ATP binding site, and the cysteine desulfurase Nfs1 is differentially oxidized at C199, which is adjacent to the pyridoxal phosphate cofactor. Future work will probe the functional consequences of Sod1-dependent protein oxidation. We also identified proteins that are more oxidized in *sod1*Δ cells, which we interpret as arising due to oxidative stress associated with the loss of GAPDH/Sod1 signaling and the concomitant decrease in NADPH levels and/or $O_2^{\bullet-}$ toxicity. It is worth noting that although past redox proteomics studies revealed much about potential targets of redox regulation, they typically involved treatment with exogenous oxidants mimicking pathological stress levels outside the physiological range (24, 77–80). Our study is notable in that we have identified redox targets of a physiological endogenous source of H_2O_2.

To what degree does Sod1 regulate thiol oxidation in animal models? A recent elegant redox proteomics study from Couchani and coworkers (81), termed "Oximouse," describes tissue specific protein thiol oxidation in a mouse model. Since active Sod1 requires the formation of an intramolecular disulfide bond between Cys-147 and Cys-56, we plotted percent Sod1-Cys147 oxidation as a proxy for mature active Sod1 against overall average Cys oxidation in each tissue and found a statistically significant linear correlation ($r^2 = 53$; $P = 0.04$) (*SI Appendix*, Fig. S12*A*). To determine if this correlation between active Sod1 and overall thiol oxidation was unique to Sod1, we also plotted tissue Cys oxidation against the oxidation of active site Cys residues in other peroxide metabolizing enzymes, including peroxiredoxins 1 and 5 (PRDX1, PRDX5) or glutaredoxin 3 (GLRX3). Unlike Sod1, the activity of these other enzymes, as assessed by their active site oxidation, do not significantly correlate with overall Cys oxidation (*SI Appendix*, Fig. S12 *B–F*). Moreover, we also found that the oxidation of other enzymes known to be redox regulated by Sod1, including tyrosine phosphatases PTP1N (PTP1B in humans) and PTPN11 (82, 83) and a GTPase involved in vesicular protein transport from the ER to the Golgi, Rab1α (84) (*SI Appendix*, Fig. S12 *G–I*), exhibit a linear correlation between active Sod1 and their active site oxidation. Notably, there is no correlation with PRDX1 Cys oxidation, which is

typically associated with the transmission of oxidizing equivalents to regulate redox signaling (59) (*SI Appendix*, Fig. S12 *J–L*). Together, the data we extracted from the Oximouse study supports our principal findings from yeast that Sod1-derived peroxide regulates proteome-wide thiol oxidation.

Our studies have also finally explained a mystery regarding the role of Sod1 in antioxidant defense. Prior to the present work, the primary role of Sod1 in antioxidant defense was thought to be $O_2^{\bullet-}$ scavenging. However, we previously found that the vast majority of Sod1 (>99%) was dispensable for protection against cell wide markers of $O_2^{\bullet-}$ toxicity (15). We surmised that exceedingly low amounts of Sod1 were sufficient to protect against $O_2^{\bullet-}$ because the targets of $O_2^{\bullet-}$ toxicity are limited in scope, primarily Fe-S cofactor-containing proteins. Indeed, all $O_2^{\bullet-}$-related toxicity phenotypes arise from diminished activity of Fe-S enzymes and iron toxicity due to iron release from damaged clusters. Our work indicates that a broader role for Sod1 in oxidant defense is to promote the production of NADPH via the GAPDH/Sod1 signaling axis. As a major cellular reductant for numerous antioxidant systems, NADPH offers more expansive protection against redox stress than just defending against $O_2^{\bullet-}$. Since GAPDH and Sod1 are among the most ancient and highly conserved enzymes in aerobic life, we propose that this reported function of Sod1 to produce NADPH via GAPDH oxidation was a key requirement for O_2 sensing and integration for adaptation to life in air.

Materials and Methods

All cell lines, culture conditions, reagents, methods, including MS-based redox proteomics, and statistical analyses are described in *SI Appendix, SI Materials and Methods*. Yeast strains used in this study were in the BY4741 genetic background and HEK293 and MCF-7 cells were obtained from American Type Culture Collection (ATCC). Plasmids and primers (*SI Appendix*, Table S1) are described in *SI Appendix, SI Materials and Methods*. The synthetic gene for HyPer7 (85) was purchased from Synbio Technologies and was codon-optimized for expression in *S. cerevisiae* (*SI Appendix*, Table S2). Published methods for immunoblotting and IP (15, 16), mPEG-mal labeling (48, 86), GAPDH activity (87), SOD activity (15, 16), Pma1 activity (16), DHE (15), and HyPer7-mediated (85) superoxide and peroxide detection, respectively, pH measurements using pHluorin (88, 89), NADPH detection (90), Sod1 silencing (40), MS-based redox proteomics (57), and cell growth were employed and are described in detail in *SI Appendix, SI Materials and Methods*.

Data Availability. All study data are included in the manuscript and/or supporting information. The mass spectrometry proteomics data have been deposited to the ProteomeXchange Consortium (91) via the PRIDE partner repository (92) with the dataset identifier PXD030372.

ACKNOWLEDGMENTS. We thank Ms. Kathrin Ulrich for assistance with mPEG-mal labeling protocols, Prof. Valeria Culotta for the Sod1 antibody, Prof. Tobias Dick for the *tdh1*Δ *tdh2*Δ *tdh3*Δ strains, Prof. Dennis Thiele for the mitochondrial targeted Sod1 allele, Prof. Michael Breitenbach for the Yno1 plasmids, and Prof. David Eide for the HA-Tsa1 constructs. We acknowledge support from the NIH grant GM118744 (to A.R.R. and M.P.T.) and the Blanchard Professorship (A.R.R.).

1. A. R. Reddi, V. C. Culotta, Regulation of manganese antioxidants by nutrient sensing pathways in *Saccharomyces cerevisiae*. *Genetics* **189**, 1261–1270 (2011).
2. H. D. Teixeira, R. I. Schumacher, R. Meneghini, Lower intracellular hydrogen peroxide levels in cells overexpressing CuZn-superoxide dismutase. *Proc. Natl. Acad. Sci. U.S.A.* **95**, 7872–7875 (1998).
3. D. H. Flint, J. F. Tuminello, M. H. Emptage, The inactivation of Fe-S cluster containing hydro-lyases by superoxide. *J. Biol. Chem.* **268**, 22369–22376 (1993).
4. S. I. Liochev, I. Fridovich, Superoxide and iron: Partners in crime. *IUBMB Life* **48**, 157–161 (1999).
5. J. A. Imlay, Pathways of oxidative damage. *Annu. Rev. Microbiol.* **57**, 395–418 (2003).
6. Y. Wang, R. Branicky, A. Noë, S. Hekimi, Superoxide dismutases: Dual roles in controlling ROS damage and regulating ROS signaling. *J. Cell Biol.* **217**, 1915–1928 (2018).
7. T. Bieliński, Z. Krawiec, A. Liczmański, J. Litwińska, Is hydroxyl radical generated by the Fenton reaction in vivo? *Biochem. Biophys. Res. Commun.* **130**, 533–539 (1985).
8. S. Elchuri *et al.*, CuZnSOD deficiency leads to persistent and widespread oxidative damage and hepatocarcinogenesis later in life. *Oncogene* **24**, 367–380 (2005).
9. E. C. Chang, D. J. Kosman, O_2-dependent methionine auxotrophy in Cu,Zn superoxide dismutase-deficient mutants of *Saccharomyces cerevisiae*. *J. Bacteriol.* **172**, 1840–1845 (1990).
10. E. B. Gralla, J. S. Valentine, Null mutants of *Saccharomyces cerevisiae* Cu,Zn superoxide dismutase: Characterization and spontaneous mutation rates. *J. Bacteriol.* **173**, 5918–5920 (1991).
11. L. A. Sturtz, V. C. Culotta, Superoxide dismutase null mutants of baker's yeast, Saccharomyces cerevisiae. *Methods Enzymol.* **349**, 167–172 (2002).
12. S. L. Liochev, The role of iron-sulfur clusters in in vivo hydroxyl radical production. *Free Radic. Res.* **25**, 369–384 (1996).
13. S. I. Liochev, I. Fridovich, The role of $O_2^{\cdot-}$ in the production of HO.: In vitro and in vivo. *Free Radic. Biol. Med.* **16**, 29–33 (1994).
14. L. B. Corson, J. Folmer, J. J. Strain, V. C. Culotta, D. W. Cleveland, Oxidative stress and iron are implicated in fragmenting vacuoles of *Saccharomyces cerevisiae* lacking Cu,Zn-superoxide dismutase. *J. Biol. Chem.* **274**, 27590–27596 (1999).
15. C. Montllor-Albalate *et al.*, Extra-mitochondrial Cu/Zn superoxide dismutase (Sod1) is dispensable for protection against oxidative stress but mediates peroxide signaling in *Saccharomyces cerevisiae*. *Redox Biol.* **21**, 101064 (2019).
16. A. R. Reddi, V. C. Culotta, SOD1 integrates signals from oxygen and glucose to repress respiration. *Cell* **152**, 224–235 (2013).
17. L. B. Poole, A. Hall, K. J. Nelson, Overview of peroxiredoxins in oxidant defense and redox regulation. *Curr. Protoc. Toxicol.* **49**, 7.9.1–7.9.15 (2011).
18. H. N. Kirkman, G. F. Gaetani, Catalase: A tetrameric enzyme with four tightly bound molecules of NADPH. *Proc. Natl. Acad. Sci. U.S.A.* **81**, 4343–4347 (1984).
19. H. N. Kirkman, S. Galiano, G. F. Gaetani, The function of catalase-bound NADPH. *J. Biol. Chem.* **262**, 660–666 (1987).
20. S. Sehati *et al.*, Metabolic alterations in yeast lacking copper-zinc superoxide dismutase. *Free Radic. Biol. Med.* **50**, 1591–1598 (2011).
21. K. H. Slekar, D. J. Kosman, V. C. Culotta, The yeast copper/zinc superoxide dismutase and the pentose phosphate pathway play overlapping roles in oxidative stress protection. *J. Biol. Chem.* **271**, 28831–28836 (1996).
22. S.-M. Jeon, Regulation and function of AMPK in physiology and diseases. *Exp. Mol. Med.* **48**, e245 (2016).
23. D. Peralta *et al.*, A proton relay enhances H_2O_2 sensitivity of GAPDH to facilitate metabolic adaptation. *Nat. Chem. Biol.* **11**, 156–163 (2015).
24. J. van der Reest, S. Lilla, L. Zheng, S. Zanivan, E. Gottlieb, Proteome-wide analysis of cysteine oxidation reveals metabolic sensitivity to redox stress. *Nat. Commun.* **9**, 1581 (2018).
25. D. Anastasiou *et al.*, Inhibition of pyruvate kinase M2 by reactive oxygen species contributes to cellular antioxidant responses. *Science* **334**, 1278–1283 (2011).
26. A. R. Mitchell *et al.*, Redox regulation of pyruvate kinase M2 by cysteine oxidation and S-nitrosation. *Biochem. J.* **475**, 3275–3291 (2018).
27. R. Kunjithapatham, S. Ganapathy-Kanniappan, GAPDH with NAD^+-binding site mutation competitively inhibits the wild-type and affects glucose metabolism in cancer. *Biochim. Biophys. Acta, Gen. Subj.* **1862**, 2555–2563 (2018).
28. J. A. Diderich, L. M. Raamsdonk, A. L. Kruckeberg, J. A. Berden, K. Van Dam, Physiological properties of *Saccharomyces cerevisiae* from which hexokinase II has been deleted. *Appl. Environ. Microbiol.* **67**, 1587–1593 (2001).
29. L. B. Bockus *et al.*, Cardiac insulin signaling regulates glycolysis through phosphofructokinase 2 content and activity. *J. Am. Heart Assoc.* **6**, e007159 (2017).
30. A. Krüger *et al.*, The pentose phosphate pathway is a metabolic redox sensor and regulates transcription during the antioxidant response. *Antioxid. Redox Signal.* **15**, 311–324 (2011).
31. M. Ralser *et al.*, Dynamic rerouting of the carbohydrate flux is key to counteracting oxidative stress. *J. Biol.* **6**, 10 (2007).
32. M. Ralser *et al.*, Metabolic reconfiguration precedes transcriptional regulation in the antioxidant response. *Nat. Biotechnol.* **27**, 604–605 (2009).
33. A. Kuehne *et al.*, Acute activation of oxidative pentose phosphate pathway as first-line response to oxidative stress in human skin cells. *Mol. Cell* **59**, 359–371 (2015).
34. E. Mullarky, L. C. Cantley, "Diverting glycolysis to combat oxidative stress" in *Innovative Medicine*, K. Nakao, N. Minato, S. Uemoto, Eds. (Springer, Tokyo, 2015), pp. 3–23.
35. D. Christodoulou *et al.*, Reserve flux capacity in the pentose phosphate pathway enables *Escherichia coli*'s rapid response to oxidative stress. *Cell Syst.* **6**, 569–578.e7 (2018).
36. A. A. Shestov *et al.*, Quantitative determinants of aerobic glycolysis identify flux through the enzyme GAPDH as a limiting step. *eLife* **3**, e03342 (2014).
37. M. V. Liberti *et al.*, A predictive model for selective targeting of the Warburg effect through GAPDH inhibition with a natural product. Cell *Metab.* **26**, 648–659.e648 (2017).
38. C. C. Winterbourn, M. B. Hampton, Thiol chemistry and specificity in redox signaling. *Free Radic. Biol. Med.* **45**, 549–561 (2008)
39. J. C. Juarez *et al.*, Superoxide dismutase 1 (SOD1) is essential for H_2O_2-mediated oxidation and inactivation of phosphatases in growth factor signaling. *Proc. Natl. Acad. Sci. U.S.A.* **105**, 7147–7152 (2008).
40. B. Chandrasekharan *et al.*, Cu/Zn superoxide dismutase (Sod1) regulates the canonical Wnt signaling pathway. *Biochem. Biophys. Res. Commun.* **534**, 720–726 (2021).
41. P. Jouhten *et al.*, Oxygen dependence of metabolic fluxes and energy generation of *Saccharomyces cerevisiae* CEN.PK113-1A. *BMC Syst. Biol.* **2**, 60 (2008).

BIOCHEMISTRY

42. R. J. Viator *et al.*, Hypoxia-induced increases in glucose uptake do not cause oxidative injury or advanced glycation end-product (AGE) formation in vascular endothelial cells. *Physiol. Rep.* **3**, e12460 (2015).
43. A. Ouiddir, C. Planès, I. Fernandes, A. VanHesse, C. Clerici, Hypoxia upregulates activity and expression of the glucose transporter GLUT1 in alveolar epithelial cells. *Am. J. Respir. Cell Mol. Biol.* **21**, 710–718 (1999).
44. B. A. Bruckner, C. V. Ammini, M. P. Otal, M. K. Raizada, P. W. Stacpoole, Regulation of brain glucose transporters by glucose and oxygen deprivation. *Metabolism* **48**, 422–431 (1999).
45. M. Tarsio, H. Zheng, A. M. Smardon, G. A. Martínez-Muñoz, P. M. Kane, Consequences of loss of Vph1 protein-containing vacuolar ATPases (V-ATPases) for overall cellular pH homeostasis. *J. Biol. Chem.* **286**, 28089–28096 (2011).
46. J. A. Baron, J. S. Chen, V. C. Culotta, Cu/Zn superoxide dismutase and the proton ATPase Pma1p of *Saccharomyces cerevisiae*. *Biochem. Biophys. Res. Commun.* **462**, 251–256 (2015).
47. D. A. Hanna *et al.*, Heme dynamics and trafficking factors revealed by genetically encoded fluorescent heme sensors. *Proc. Natl. Acad. Sci. U.S.A.* **113**, 7539–7544 (2016).
48. L. A. G. van Leeuwen, E. C. Hinchy, M. P. Murphy, E. L. Robb, H. M. Cochemé, Click-PEGylation—A mobility shift approach to assess the redox state of cysteines in candidate proteins. *Free Radic. Biol. Med.* **108**, 374–382 (2017).
49. N. Brandes, D. Reichmann, H. Tienson, L. I. Leichert, U. Jakob, Using quantitative redox proteomics to dissect the yeast redoxome. *J. Biol. Chem.* **286**, 41893–41903 (2011).
50. L. K. Wood, D. J. Thiele, Transcriptional activation in yeast in response to copper deficiency involves copper-zinc superoxide dismutase. *J. Biol. Chem.* **284**, 404–413 (2009).
51. M. Rinnerthaler *et al.*, Yno1p/Aim14p, a NADPH-oxidase ortholog, controls extramitochondrial reactive oxygen species generation, apoptosis, and actin cable formation in yeast. *Proc. Natl. Acad. Sci. U.S.A.* **109**, 8658–8663 (2012).
52. N. M. Brown, A. S. Torres, P. E. Doan, T. V. O'Halloran, Oxygen and the copper chaperone CCS regulate posttranslational activation of Cu,Zn superoxide dismutase. *Proc. Natl. Acad. Sci. U.S.A.* **101**, 5518–5523 (2004).
53. J. M. Leitch *et al.*, Activation of Cu,Zn-superoxide dismutase in the absence of oxygen and the copper chaperone CCS. *J. Biol. Chem.* **284**, 21863–21871 (2009).
54. J. M. Leitch *et al.*, Post-translational modification of Cu/Zn superoxide dismutase under anaerobic conditions. *Biochemistry* **51**, 677–685 (2012).
55. C. White *et al.*, Copper transport into the secretory pathway is regulated by oxygen in macrophages. *J. Cell Sci.* **122**, 1315–1321 (2009).
56. L. Papa, M. Hahn, E. L. Marsh, B. S. Evans, D. Germain, SOD2 to SOD1 switch in breast cancer. *J. Biol. Chem.* **289**, 5412–5416 (2014).
57. M. Vajrychova *et al.*, Quantification of cellular protein and redox imbalance using SILAC-iodoTMT methodology. *Redox Biol.* **24**, 101227 (2019).
58. B. Ho, A. Baryshnikova, G. W. Brown, Unification of protein abundance datasets yields a quantitative *Saccharomyces cerevisiae* proteome. *Cell Syst.* **6**, 192–205.e3 (2018).
59. S. Stöcker, M. Maurer, T. Ruppert, T. P. Dick, A role for 2-Cys peroxiredoxins in facilitating cytosolic protein thiol oxidation. *Nat. Chem. Biol.* **14**, 148–155 (2018).
60. Z. A. Wood, L. B. Poole, P. A. Karplus, Peroxiredoxin evolution and the regulation of hydrogen peroxide signaling. *Science* **300**, 650–653 (2003).
61. C. J. Banks, J. L. Andersen, Mechanisms of SOD1 regulation by post-translational modifications. *Redox Biol.* **26**, 101270 (2019).
62. C. J. Banks *et al.*, Acylation of superoxide dismutase 1 (SOD1) at K122 governs SOD1-mediated inhibition of mitochondrial respiration. *Mol. Cell. Biol.* **37**, e00354-17 (2017).
63. C. K. Tsang, Y. Liu, J. Thomas, Y. Zhang, X. F. S. Zheng, Superoxide dismutase 1 acts as a nuclear transcription factor to regulate oxidative stress resistance. *Nat. Commun.* **5**, 3446 (2014).
64. C. K. Tsang *et al.*, SOD1 phosphorylation by mTORC1 couples nutrient sensing and redox regulation. *Mol. Cell* **70**, 502–515.e8 (2018).
65. C.-L. Liu *et al.*, Targeting the pentose phosphate pathway increases reactive oxygen species and induces apoptosis in thyroid cancer cells. *Mol. Cell. Endocrinol.* **499**, 110595 (2020).
66. M. L. Gomez, N. Shah, T. C. Kenny, E. C. Jenkins Jr, D. Germain, SOD1 is essential for oncogene-driven mammary tumor formation but dispensable for normal development and proliferation. *Oncogene* **38**, 5751–5765 (2019).
67. R. Somwar *et al.*, Superoxide dismutase 1 (SOD1) is a target for a small molecule identified in a screen for inhibitors of the growth of lung adenocarcinoma cell lines. *Proc. Natl. Acad. Sci. U.S.A.* **108**, 16375–16380 (2011).
68. P. Huang, L. Feng, E. A. Oldham, M. J. Keating, W. Plunkett, Superoxide dismutase as a target for the selective killing of cancer cells. *Nature* **407**, 390–395 (2000).
69. J. C. Juarez *et al.*, Copper binding by tetrathiomolybdate attenuates angiogenesis and tumor cell proliferation through the inhibition of superoxide dismutase 1. *Clin. Cancer Res.* **12**, 4974–4982 (2006).
70. N. Hempel, T. R. Bartling, B. Mian, J. A. Melendez, Acquisition of the metastatic phenotype is accompanied by H_2O_2-dependent activation of the p130Cas signaling complex. *Mol. Cancer Res.* **11**, 303–312 (2013).
71. N. Hempel, P. M Carrico, J. A. Melendez, Manganese superoxide dismutase (Sod2) and redox-control of signaling events that drive metastasis. *Anticancer Agents Med. Chem* **11**, 191–201 (2011).
72. K. M. Connor *et al.*, Manganese superoxide dismutase enhances the invasive and migratory activity of tumor cells. *Cancer Res.* **67**, 10260–10267 (2007).
73. P. C. Hart *et al.*, MnSOD upregulation sustains the Warburg effect via mitochondrial ROS and AMPK-dependent signalling in cancer. *Nat. Commun.* **6**, 6053 (2015).
74. F. L. Muller, Y. Liu, H. Van Remmen, Complex III releases superoxide to both sides of the inner mitochondrial membrane. *J. Biol. Chem.* **279**, 49064–49073 (2004).
75. D. Han, F. Antunes, R. Canali, D. Rettori, E. Cadenas, Voltage-dependent anion channels control the release of the superoxide anion from mitochondria to cytosol. *J. Biol. Chem.* **278**, 5557–5563 (2003).
76. N. S. Chandel *et al.*, Mitochondrial reactive oxygen species trigger hypoxia-induced transcription. *Proc. Natl. Acad. Sci. U.S.A.* **95**, 11715–11720 (1998).
77. K. Araki *et al.*, Redox sensitivities of global cellular cysteine residues under reductive and oxidative stress. *J. Proteome Res.* **15**, 2548–2559 (2016).
78. U. Topf *et al.*, Quantitative proteomics identifies redox switches for global translation modulation by mitochondrially produced reactive oxygen species. *Nat. Commun.* **9**, 324 (2018).
79. L. I. Leichert *et al.*, Quantifying changes in the thiol redox proteome upon oxidative stress in vivo. *Proc. Natl. Acad. Sci. U.S.A.* **105**, 8197–8202 (2008).
80. L. Fu *et al.*, Systematic and quantitative assessment of hydrogen peroxide reactivity with cysteines across human proteomes. *Mol. Cell. Proteomics* **16**, 1815–1828 (2017).
81. H. Xiao *et al.*, A quantitative tissue-specific landscape of protein redox regulation during aging. *Cell* **180**, 968–983.e24 (2020).
82. N. K. Tonks, Protein tyrosine phosphatases: From genes, to function, to disease. *Nat. Rev. Mol. Cell Biol.* **7**, 833–846 (2006).
83. S.-R. Lee, K.-S. Kwon, S.-R. Kim, S. G. Rhee, Reversible inactivation of protein-tyrosine phosphatase 1B in A431 cells stimulated with epidermal growth factor. *J. Biol. Chem.* **273**, 15366–15372 (1998).
84. S. E. Leonard, K. G. Reddie, K. S. Carroll, Mining the thiol proteome for sulfenic acid modifications reveals new targets for oxidation in cells. *ACS Chem. Biol.* **4**, 783–799 (2009).
85. V. V. Pak *et al.*, Ultrasensitive genetically encoded indicator for hydrogen peroxide identifies roles for the oxidant in cell migration and mitochondrial function. *Cell Metab.* **31**, 642–653.e6 (2020).
86. C. Chen *et al.*, Identification of a disulfide bridge in sodium-coupled neutral amino acid transporter 2(SNAT2) by chemical modification. *PLoS One* **11**, e0158319 (2016).
87. Y. Li, J. H. Kim, E. H. Choi, I. Han, Promotion of osteogenic differentiation by non-thermal biocompatible plasma treated chitosan scaffold. *Sci. Rep.* **9**, 3712 (2019).
88. G. Miesenböck, D. A. De Angelis, J. E. Rothman, Visualizing secretion and synaptic transmission with pH-sensitive green fluorescent proteins. *Nature* **394**, 192–195 (1998).
89. R. Orij, J. Postmus, A. Ter Beek, S. Brul, G. J. Smits, In vivo measurement of cytosolic and mitochondrial pH using a pH-sensitive GFP derivative in *Saccharomyces cerevisiae* reveals a relation between intracellular pH and growth. *Microbiology (Reading)* **155**, 268–278 (2009).
90. L. Li *et al.*, TAp73-induced phosphofructokinase-1 transcription promotes the Warburg effect and enhances cell proliferation. *Nat. Commun.* **9**, 4683 (2018).
91. E. W. Deutsch *et al.*, The ProteomeXchange consortium in 2020: Enabling 'big data' approaches in proteomics. *Nucleic Acids Res.* **48**, D1145–D1152 (2020).
92. Y. Perez-Riverol *et al.*, The PRIDE database and related tools and resources in 2019: improving support for quantification data. *Nucleic Acids Res.* **47**, D442–D450 (2019).